



High-performance Pd–Au bimetallic catalyst with mesoporous silica nanoparticles as support and its catalysis of cinnamaldehyde hydrogenation

Xu Yang^{a,b}, Dan Chen^{a,b}, Shijun Liao^{a,b,*}, Huiyu Song^{a,b}, Yingwei Li^{a,b}, Zhiyong Fu^{a,b}, Yunlan Su^c

^a School of Chemistry and Chemical Engineering, South China University of Technology, Guangzhou 510641, China

^b Key Lab for Fuel Cell Technology of Guangdong Province & Key Lab of Enhanced Heat Transfer and Energy Conservation, Ministry of Education, China

^c Institute of Chemistry, Chinese Academy of Sciences, Beijing 100191, China

ARTICLE INFO

Article history:

Received 3 February 2012

Revised 3 April 2012

Accepted 4 April 2012

Available online 22 May 2012

Keywords:

Bimetallic

Cinnamaldehyde hydrogenation

Mesoporous silica

Pd–Au

Synergistic effect

ABSTRACT

A high-performance bimetallic catalyst with mesoporous silica nanoparticles as support, PdAu/MSN, was prepared by an organic impregnation–hydrogen reduction approach. A series of investigations were conducted to assess the effects of (i) the porous nanoparticle support on the dispersion of active components and on the catalyst's performance, (ii) the addition of gold on the dispersion of active components and the catalyst's activity, and (iii) the preparation parameters, such as solvent, pressure, and temperature, on the catalyst's activity. The active metallic components were highly dispersed, with particle size 2.5 nm. The addition of gold to the catalyst favorably promoted the hydrogenation of cinnamaldehyde. The activity of PdAu_{0.2}/MSN (with Au/Pd molar ratio 0.2:1) was up to four times higher than that of Pd/MSN (without Au as a promoter) and eight times higher than that of commercial Pd/C catalyst. The enhanced activity of PdAu_{0.2}/MSN can be attributed to the synergistic effect of Pd with the added Au and the highly dispersed active components. The ultrahigh activity, as well as its novel structure with controllable compositions, makes this catalyst very attractive for both fundamental research and practical applications.

© 2012 Elsevier Inc. All rights reserved.

1. Introduction

In green chemistry [1,2], achieving high dispersion of a supported noble metal catalyst (e.g., Pd, Au, Pt) has been a significant issue in the field of heterogeneous catalysis [3–6], due to these catalysts' inherent high activity but high cost. However, it is well known that during the activation process (calcination or hydrogen reduction), some of the noble metals, especially palladium and gold, are easily reduced and are apt to form large metal particles, due to the unique physical/chemical properties of noble metals (autocatalysis, mobility, and so on), resulting in poor metal dispersion and low activity. Thus, preparing a high-performance, heterogeneous noble metal catalyst with high dispersion of the active components has been an ongoing challenge.

Alloying with a second metal has proved effective for obtaining a high-activity catalyst, especially for Pd-based catalysts, as reported in several studies [7–11]. The promotion effect of alloying not only improves resistance to particle sintering [8] but also modifies the geometry and electronic properties of the active species. For example, Hutchings' group reported a TiO₂-supported bimetallic catalyst with a Pd-rich shell and an Au-rich core that showed superior catalytic performance for the selective oxidation

of alcohol (TOFs up to 270,000 h⁻¹) [12,13] and the direct synthesis of H₂O₂ [14,15]; recently, they extended the catalyst's applications to oxidation of the primary C–H bond [16]. Venezia and coworkers [17–19] prepared PdAu catalysts with varied Au/Pd ratios for the hydrodesulfurization of aromatic compounds and found that adding Au could modify the substrate's adsorption model. Goodman's [11,20], as well as Prati's group [9], investigated the ensemble effect of Pd monomer isolated by Au, which showed unique properties for the synthesis of vinyl acetate and glycerol oxidation, respectively. Zhao's group found that physically mixed TiO₂-supported Pd and Au catalysts can accelerate the hydrogen spillover process [10].

Mesoporous silica (MS) has gained intense interest in the field of nanomaterials and catalysis [21–24]. It is an ideal support candidate for the preparation of high-dispersion catalysts, based on its unique advantages over conventional support materials: (i) high surface area and pore volume facilitate the adsorption and dispersion of metal salt via the impregnation method, avoiding the addition of the acid/base organic polymer required for precipitation–deposition or other complicated methods [25]; (ii) intrinsic porosity provides more access to the active center for the substrate [26]; (iii) mesoporous channels trap active metal particles that can resist deactivation during reaction [21,27]; and most importantly from another point of view, (iv) inactive siliceous properties make it an ideal support for investigating the interaction between active components, with less interruption by metal–support interaction [28].

* Corresponding author at: School of Chemistry and Chemical Engineering, South China University of Technology, Guangzhou 510641, China.

E-mail address: chsjliao@scut.edu.cn (S. Liao).

The cinnamaldehyde (CALD) hydrogenation route, depicted in Scheme 1, can result in various product distributions, depending on the active metal, solvent, and promoter [29–32]. Gallezot and Richard reported [33] that a Pd catalyst favored the production of hydrocinnamaldehyde (HALD), while a Pt-based catalyst facilitated the production of cinnamyl alcohol, both of which are important intermediates in the preparation of pharmaceuticals [34]. To date, most published research has applied mono-Pt or modified Pt catalysts for selective hydrogenation of CALD to cinnamyl alcohol, and few reports have involved the utilization of PdAu bimetallic catalysts for producing HALD.

In this paper, we extended our previous work using mesoporous silica nanoparticles (MSNs) as supports [35] and prepared a series of high-performance bimetallic catalysts, PdAu/MSN. We found that under mild conditions, adding Au and using MSN as a support greatly enhanced Pd dispersion and the catalyst's performance toward selective hydrogenation of CALD to HALD. The effect of metal composition on the catalyst's structure and behavior was investigated to explore the intrinsic alloy synergistic effect.

2. Experimental

2.1. Catalyst preparation

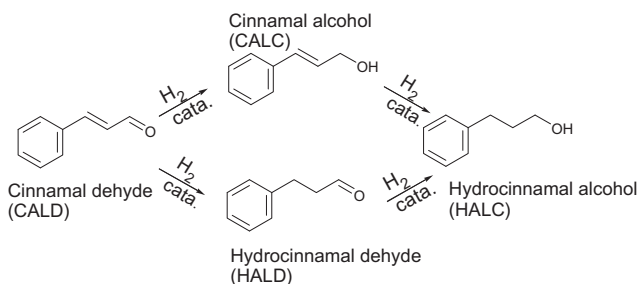
Mesoporous silica nanoparticles were prepared according to a typical MCM-41 synthesis route [36]: 0.25 g CTABr was dissolved in 100 ml deionized water under mild stirring. After the addition of ammonium solution (25 wt.%), TEOS was added dropwise to obtain a final mixture composition of 0.051CTABr : 414-H₂O : 3.29NH₃ : 1TEOS. After 10 h of stirring, white precipitates were obtained and then filtered, washed, dried, and calcined at 600 °C for 4 h to remove the residual template.

PdAu bimetallic catalysts were prepared according to the procedures we reported previously [35]. First, the MSN silica support was pretreated in a muffle oven at 200 °C for 2 h and then was impregnated with an ethanol solution of PdCl₂ and HAuCl₄, at various Au/Pd molar ratios, at room temperature under stirring. The solvent was then evaporated in a water bath at 70 °C, with further vacuum drying at 40 °C for 12 h. The PdAu/MSN catalyst was finally prepared by reducing the sample for 2 h under hydrogen flow at 200 °C in a tubular furnace with programmed temperature control, at a rate of 3 °C min⁻¹.

Three catalyst samples were prepared, with Au/Pd molar ratios of 0.1, 0.2, and 0.4, respectively. For comparison, Au/MSN and Pd/MSN were prepared using the same procedures. The basic specifications of all five catalyst samples are listed in Table 1.

2.2. Catalyst characterization

X-ray diffraction (XRD) patterns were obtained with a D/max-III A X-ray diffractometer (Rigaku, Japan) using CuK α radiation (35 kV, 30 mA) at a rate of 0.5 °C min⁻¹.



Scheme 1. Selective hydrogenation of cinnamaldehyde.

Atomic absorption analysis (AAS) was performed with a SpectrAA-220Z (Varian, USA).

The N₂ adsorption–desorption isotherms were measured with a Tristar 3010 isothermal nitrogen sorption analyzer (Micromeritics, USA) using a continuous-adsorption procedure.

H₂ chemisorption was measured according to a previously reported method [37]. The measurement was performed at 298 K in a standard volumetric glass apparatus from Belsorp-HP (Ankersmid, Netherlands). The double isotherm method was used to determine the amount of irreversibly adsorbed hydrogen, which allows calculation of the apparent metallic dispersion (H/Pd), assuming an adsorption stoichiometry of H:Pd = 1:1. The amount of chemisorbed hydrogen was determined by extrapolating the leaner part of the isotherms to zero pressure.

Scanning transmission electron microscopy (STEM) and high-resolution transmission electron microscopy (HRTEM) were carried out with a JEOL JEM2010 microscope (JEOL, Japan) under an accelerating voltage of 200 kV.

X-ray photoelectron spectroscopy (XPS) with an AXIS Ultra DLD (Kratos, Britain) was used to examine the catalysts' electronic properties. The binding energies were calibrated using a C1s binding energy of 284.8 eV. The peaks were fitted by a nonlinear least square fitting program using a properly weighted sum of Lorentzian and Gaussian component curves after background subtraction, according to Shirley and Sherwood.

H₂ TPR was performed on an AutoChem II 2920 chemisorption analyzer (Micromeritics, USA): a sample of 50 mg was heated from room temperature to 600 °C at a rate of 10 °C min⁻¹ in 5% H₂/Ar (40 ml min⁻¹, STP).

2.3. Catalyst evaluation

The hydrogenation of CALD was used for the hydrogenation model reaction. The reaction mixture, composed of 20–50 mg catalyst, 1.0 g CALD, and 10 ml solvent, was introduced into a 50-ml autoclave under stirring at 1000 rpm, a value chosen to eliminate the mass transfer limitation. Air in the autoclave was purged by hydrogen for 20 min, and then the reaction proceeded at the required temperature (50–100 °C) and at 0.5 MPa of 99.99% pure hydrogen.

The products were analyzed using a gas chromatograph (Agilent 6840N, USA) equipped with a FID detector. A GC–MS analyzer (Shimadzu GCMS-QP5050A, Japan), equipped with a 0.25 mm × 30 m DB-WAX capillary column, was used for the identification of products. The column oven temperature was programmed from 120 °C (held for 1 min) to 280 °C at a rate of 20 °C min⁻¹.

3. Results and discussion

3.1. Catalyst characterizations

3.1.1. XRD analysis

Fig. 1 shows the small-angle XRD patterns for the PdAu/MSN catalyst samples and the MSN sample. All of the samples, including the pristine MSN support and the metal-loaded catalysts, exhibited a very strong main peak and three other peaks in the small-angle domain, indexed as (100), (110), (200), and (210), which are reflections of the typical hexagonal mesophase p6mm, demonstrating the high quality of mesopore packing [36]. The ordered mesopores contributed to the high surface area and pore volume of the MSN support, qualities that can be beneficial to the adsorption of metal salt during impregnation and to the improvement of metal dispersion. The mesoporous properties of the samples are given in Table 1.

Table 1
Composition and porosity parameters of MSN and PdAu/MSN with various Au/Pd molar ratios.

Catalyst	Metal loading (wt.%) ^a	S _{BET} (m ² g ⁻¹) ^b	Pore size (nm) ^b	Pore volume (cm ³ g ⁻¹) ^b
Pd/C	Pd, 2.0 (1.7)	241	—	—
Pd/MSN	Pd, 2.0 (1.9)	624	3.1	1.20
PdAu _{0.1} /MSN	Pd, 2.0 (1.9) Au, 0.37 (0.35)	617	3.2	1.21
PdAu _{0.2} /MSN	Pd, 2.0 (1.9) Au, 0.74 (0.73)	622	3.1	1.19
PdAu _{0.4} /MSN	Pd, 2.0 (1.9) Au, 1.48 (1.40)	616	3.0	1.13
Au/MSN	Au, 2.0 (1.8)	620	3.1	1.17

^a The recipe metal content and the content measured by atomic absorption spectroscopy (in parentheses).

^b Derived from nitrogen adsorption–desorption isotherm.

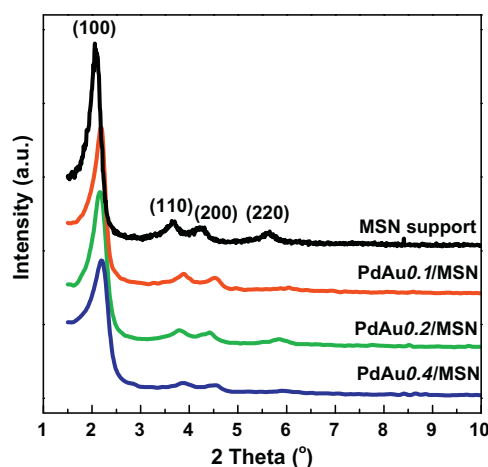


Fig. 1. Small-angle XRD patterns of MSN support and PdAu/MSN catalysts.

The metal crystallites of the catalysts were characterized using wide-angle XRD, as shown in Fig. 2a. Although the reduction temperature was low (200 °C), all of the catalyst samples exhibited three clear diffraction peaks, indexed as the (111), (110), and (220) planes of a face-centered cubic structure, indicating that all the metal components were well reduced and supported on the MSN supports. Compared with Pd/MSN and Au/MSN, all three PdAu/MSN catalysts showed a broadened diffraction peak for Pd (111) between 38° and 40°, implying that the addition of Au improved the dispersion of Pd on the MSN support and achieved smaller metal particle size. Table 2 presents all the particle size data, calculated using the Scherrer equation. The particle size decreased from 12.8 to 9.3 nm when MSN was used as the support instead of active carbon. Adding Au also sharply improved the dispersion of the active components; after just a small addition of Au (PdAu_{0.1}/MSN), the particle size decreased from 9.3 to 3.2 nm. The optimal Au/Pd molar ratio was 0.2, yielding the smallest size (3.1 nm). Although the high surface area of MSN is helpful for getting a high dispersion of palladium, it is clear that the addition of gold played a crucial role for enhancing the dispersion and decreasing the particle size of active components.

From the enlarged regional pattern between 30° and 50° (see Fig. 2b), it can be observed that when the Au/Pd ratio was increased from 0 to 0.4, the reflection peak of the samples shifted toward a lower angle, from 40.06° to 38.28° (see Table 2), implying that the metal crystallite changed from “Pd-like” to “Au-like,” or indicating PdAu alloy formation [38–40].

3.1.2. Hydrogen chemisorption

The hydrogen chemisorption results are presented in Table 2. Hydrogen can be dissociatively adsorbed onto the surface or

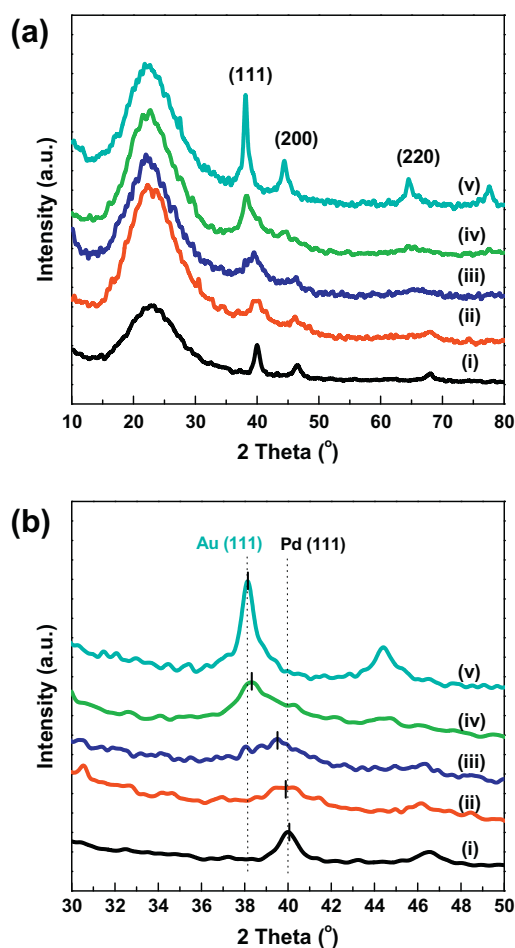


Fig. 2. XRD patterns (a) and enlarged regional patterns (b) between 30° and 50° for the catalysts (i) Pd/MSN, (ii) PdAu_{0.1}/MSN, (iii) PdAu_{0.2}/MSN, (iv) PdAu_{0.4}/MSN, and (v) Au/MSN.

Table 2
Specifications of several catalysts prepared with various metal compositions.

Catalyst	Hydrogen chemisorption		d ₍₁₁₁₎ ^a	D _{XRD} ^a	D _{TEM} ^b
	V _{irre} (μmol/g)	Dispersion			
Pd/C	0.015	0.08	—	12.8	—
Pd/MSN	0.022	0.12	40.06	9.3	6.2
PdAu _{0.1} /MSN	0.085	0.45	39.92	3.2	2.8
PdAu _{0.2} /MSN	0.100	0.53	39.51	3.1	2.5
PdAu _{0.4} /MSN	0.058	0.31	38.28	4.5	4.0

^a Calculated from XRD patterns with Jade software.

^b Average values calculated from 200 individual crystallites in TEM images.

absorbed into the Pd metal bulk. The dispersion value derived from the hydrogen chemisorption value, therefore, does not reflect the actual exposed Pd surface; however, the increasing trend in hydrogen adsorption for all five samples is quite consistent with the decreasing trend in particle size. The relatively low hydrogen adsorption for Pd/C and Pd/MSN can be attributed to their low metal dispersions, as discussed above. For the bimetallic samples, their higher irreversible hydrogen adsorption amounts compared with the mono-Pd catalyst varied with the Au/Pd ratios, in the sequence $\text{PdAu}_{0.4} < \text{PdAu}_{0.1} < \text{PdAu}_{0.2}$.

Considering the deviation of particle sizes determined by XRD method, we can say that the adsorption of hydrogen is inversely proportional to the particle size, although the hydrogen not only can be adsorbed onto the surface of palladium, but also can be dissolved into the lattice of palladium crystal. As we will discuss later, the sequence of hydrogen adsorption of three catalysts is actually quite consistent with that of their catalytic activities.

3.1.3. TEM/STEM image analysis

Typical TEM images of the mono- and bimetallic catalysts are presented in Fig. 3. Fig. 3a shows the MSN support as a monodisperse elliptical form (~ 100 nm) with honeycomb-like porosity, characteristic of typical hexagonal packing mesopores for MCM-41 family molecular sieves, which is consistent with the results from small-angle XRD analysis.

The metal dispersion of the loaded catalysts can be seen clearly from the TEM images. The mono-Pd/MSN exhibited polydispersity,

with particle sizes ranging from 1 to 10 nm (see Fig. 3b); even some larger Pd aggregations (>10 nm) can be seen, implying the sintering or aggregation of the active metal component in this catalyst, actually the aggregation of pure palladium catalyst has been recognized and reported previously by many researchers [35,41]. All of the other bimetallic catalysts showed homogeneous metal dispersion, with particle sizes of ca. <5 nm (Fig. 3c–d), demonstrating that particle size can be controlled effectively by the addition of appropriate amounts of Au. Once the ratio of Au/Pd goes up to 0.4 ($\text{PdAu}_{0.4}/\text{MSN}$), the metal particles seem to become larger, which agrees well with the XRD results. It should be noted that the average particle sizes observed from the TEM images are consistent with the values derived from the XRD data with the Scherrer equation, except for mono-Pd/MSN. This discrepancy can be ascribed to the polydispersity of Pd/MSN [41]; a comprehensive explanation can be found in Natter et al. [42].

$\text{PdAu}_{0.2}/\text{MSN}$ was observed further using STEM and HRTEM, as presented in Fig. 4. Highly dispersed metal particles trapped in the mesochannels of the MSN can be observed in Fig. 4a and b. Some of the metal nanoparticles are arranged in lines (indicated by the red arrows in Fig. 4b), or stuck in the pore's end (Fig. 4c), observed from the direction perpendicular or parallel to the mesochannel, respectively. It was reported previously that active metal particles confined in the channels of mesopores could result in some interesting nanoscale effects, such as sintering resistance [26] and low metal melting point [43]. The former property can improve the catalyst's recyclability and the latter, we assume, could

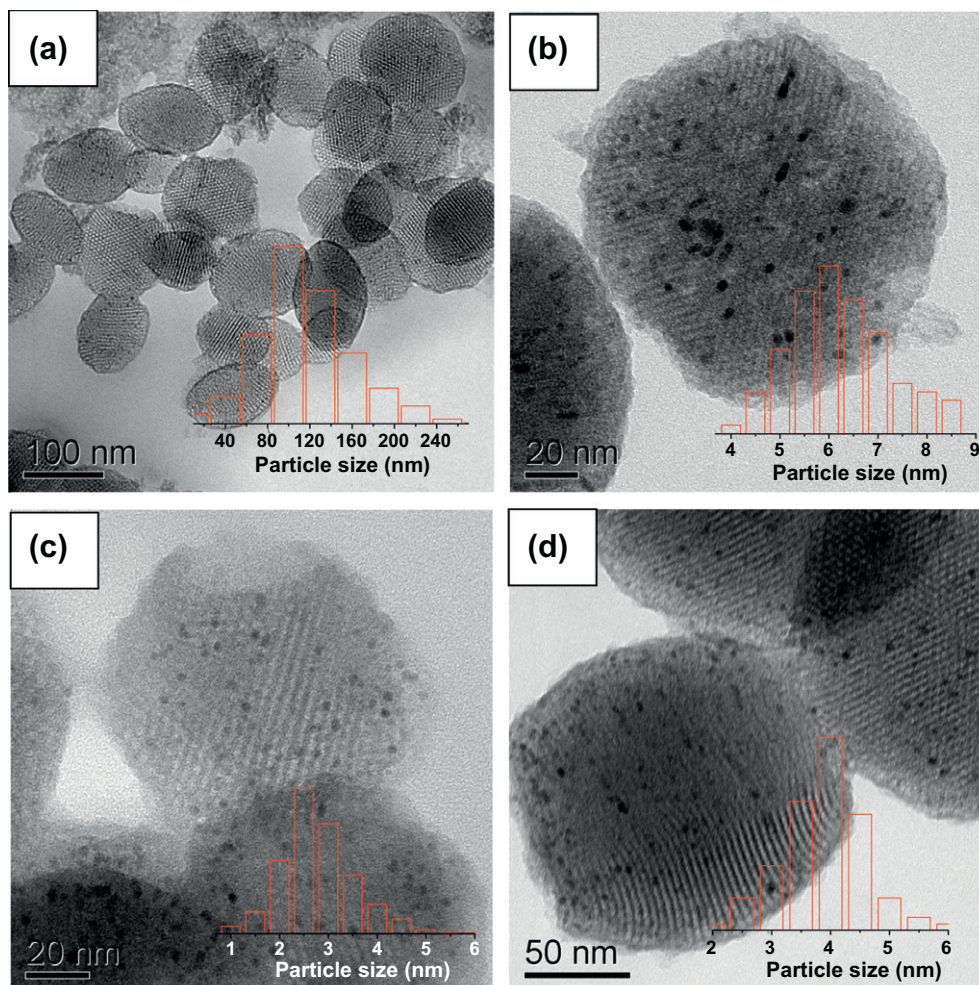


Fig. 3. HRTEM images of (a) MSN, (b) Pd/MSN, (c) PdAu_{0.1}/MSN, and (d) PdAu_{0.4}/MSN catalysts.

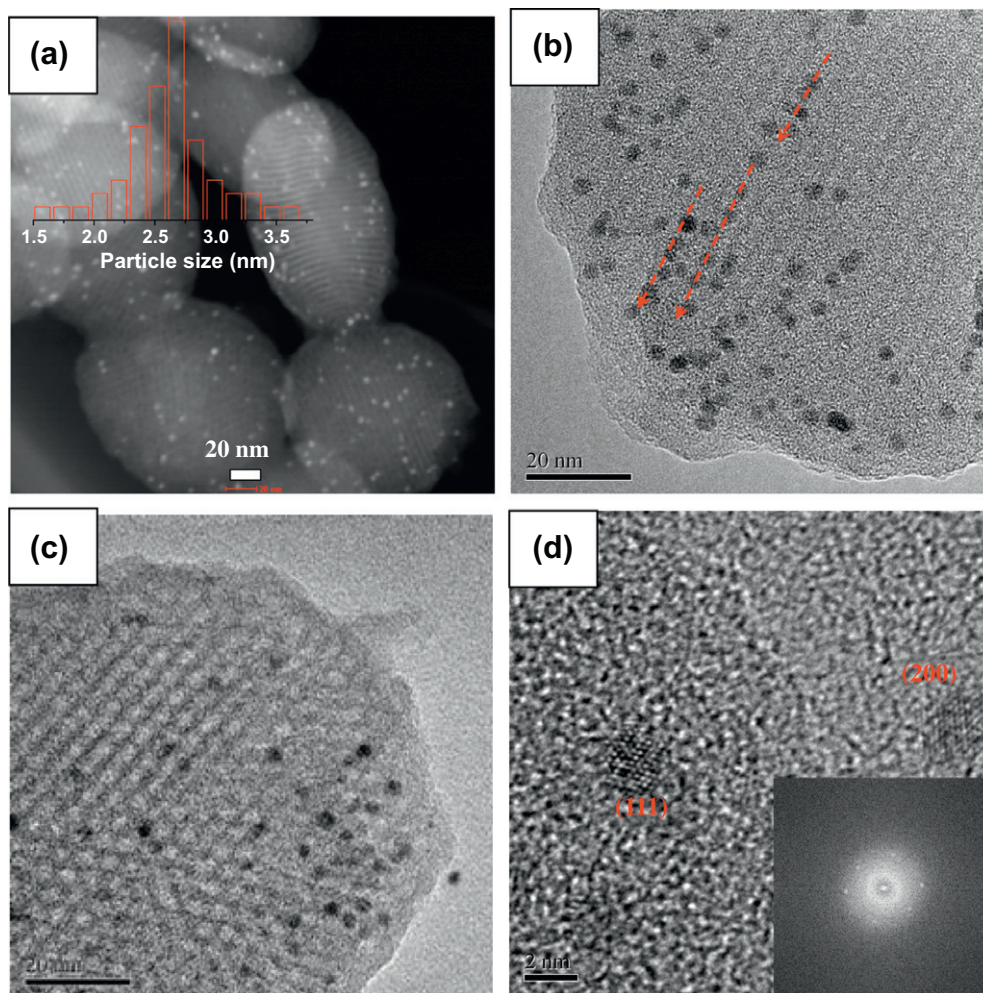


Fig. 4. STEM (a) and HRTEM (b–d) images, with corresponding electron diffraction pattern (inset in d) of the optimized PdAu_{0.2}/MSN.

be beneficial for the homogeneous alloying of metals during thermal treatment. The lattice of the (111) and (200) crystal planes can be seen in the magnified HRTEM image in Fig. 4d. Due to the equipment's detection limitations, we could not identify alloy formation from changes in the lattice.

The above observations and analysis demonstrate that the promotion of Au, as well as the high surface area of the MSN support, effectively improved the dispersion of metal components and that the Au/Pd ratio is another important factor in controlling the final particle size. Higher metal dispersion means higher exposed metal surface areas and consequently higher catalytic activity.

3.1.4. XPS analysis

The surface properties and the chemical states of Pd and Au were investigated by X-ray photoelectron spectroscopy (XPS). The Pd3d spectra of the catalysts were fitted by two doublets attributed to the higher Pd3d energy value of Pd^{II}O (>336.6 eV) and the lower energy value of metallic Pd⁰ (<335.8 eV), as shown in Fig. 5a. A shift of ca. 0.6–0.8 eV toward high binding energy with respect to the sample of monometallic Pd (335.1 eV) was observed for all three PdAu bimetallic catalysts, which is attributable to charge transfer between Au and Pd [10,39], indicating that the electronic structure of the surface Pd atoms was modified upon the addition of Au. Gold binding energies, ca. 84.1 eV, are typical of the metallic state shown in Fig. 5b.

The XPS-derived atomic ratios of Pd/Si and Au/Pd, reported in Table 3, give evidence of the surface metal composition induced

by the addition of Au. The Pd/Si ratio is close to the nominal ratio, but the Au/Pd ratio is not. It was found that, depending on the amount of Au added, the XPS-derived Au/Pd ratio varied from smaller to larger than the nominal value (see Table 3). The surface composition of an alloy can be related to the inherent microstructure of a catalyst, such as core-shell structure or homogeneous/heterogeneous alloy.

The deviation of nanoparticle PdAu catalysts has been investigated by Hutchings et al. [44] with XPS and HRTEM-XEDS. For a carbon-supported PdAu catalyst they prepared with a sol immobilization technique, it was disclosed that the smaller particles are Au-rich, whereas the larger ones tend to be Pd-rich. It also mentioned that these results are diametrically opposite to those obtained for PdAu nanoparticles prepared with impregnation methods, which was reported by Kiely and coworkers [45], implying that the deviation trend may be affected strongly by the preparation method.

Although the detection depth of XPS is up to 10 nm, which is larger than the particle sizes of the PdAu nanoparticles we prepared, we believe the XPS results may strongly reflect the microstructure and surface composition information for nanoparticles. For the sample PdAu_{0.1}/MSN, the XPS-detected ratio of Au/Pd is only 40% of the nominal ratio, but for the sample PdAu_{0.4}/MSN, this value is up to 140%, while it is 80% for PdAu_{0.2}/MSN. The more gold is added, the greater the deviation is. Combined with the results of XRD, in which the patterns changed gradually from a Pd-like pattern for PdAu_{0.1}/MSN to an Au-like pattern for PdAu_{0.4}/MSN,

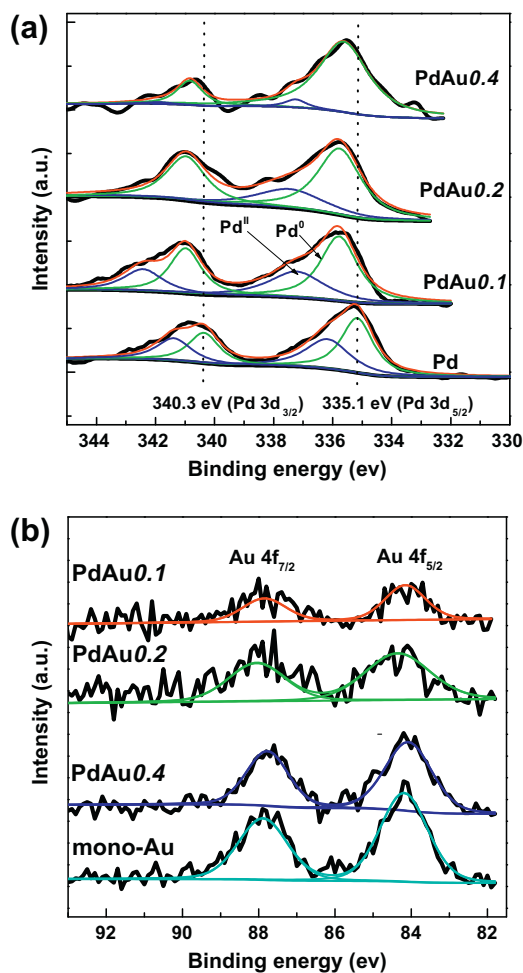


Fig. 5. XPS spectra of Pd (a) and Au (b) in the different catalysts.

Table 3

XPS Pd and Au binding energies (eV) and surface atomic ratios of the catalysts after reduction at 200 °C.

Catalyst	Binding energy (eV)		Atomic ratio	
	Pd3d _{5/2} ^a	Au4f _{7/2}	Pd/Si ($\times 10^{-3}$)	Au/Pd ^b
Pd/MSN	335.1 (0.54) [*] 336.2 (0.46)	–	4.3	–
PdAu _{0.1} /MSN	335.7 (0.63) 337.2 (0.37)	84.2	4.2	0.04 (0.10)
PdAu _{0.2} /MSN	335.8 (0.72) 337.5 (0.29)	84.3	4.4	0.16 (0.21)
PdAu _{0.4} /MSN	335.6 (0.88) 337.2 (0.12)	84.1	4.2	0.56 (0.40)
Au/MSN	–	84.1	–	–

^a For every sample, line 1 and line 2 present the binding energy of Pd3d_{5/2} of Pd and PdO, respectively, derived from XPS spectrum of the sample with XPS analysis software, and the datum in parentheses is the relative fraction of Pd or PdO in the sample.

^b The atomic ratio of Au/Pd measured by XPS, and the datum in parentheses is the ratio value measured by atomic absorption spectroscopy.

we assume that the microstructure of the PdAu alloy catalyst can be tuned by the Au/Pd ratio, and it seems that as more Au is added, upon hydrogen reduction at 200 °C, the catalyst is prone to form Au-rich surface ensembles or clusters. However, further study is still needed to disclose the mechanism of transformation of the microstructure of PdAu nanoparticles, as well as to establish a clearer correlation between the catalyst's surface composition and activity.

In addition, the fraction of Pd^{II} to metallic Pd⁰ species in the sample can be reflected roughly by the peak-fitting method. It is worth noting that increasing the Au/Pd ratio also increased the metallic Pd⁰ content with respect to the Pd^{II} species content (PdCl₂ or PdO) from 63% to 88%, seeing Table 3, which is consistent with the findings of Qian and Huang [46], confirming that adding Au may be helpful to the reduction of Pd^{II} to metallic Pd, or the protection of Pd⁰ from to be oxidized into Pd^{II}.

3.1.5. H₂ TPR analysis

To further understand the interaction between Pd and Au, as well as between the metals and the support, we investigated the reducibility of the precursor samples using hydrogen temperature program reduction (H₂ TPR). In Fig. 6, the mono-Pd catalyst precursor presents a single negative peak at 62 °C, caused by dissociation of palladium hydride [47], indicating the easy reducibility of Pd²⁺ or PdO species. The mono-Au catalyst precursor shows a broadened hydrogen consumption peak in the temperature range 130–210 °C, which could be ascribed to the reduction of Au³⁺ interacting with the SiO₂ support, with different interaction strengths [46]. For the PdAu bimetallic catalyst precursor, a sharp hydrogen consumption peak was observed, which shifted from 98 to 125 °C depending on the Au/Pd ratio, revealing that interactions occurred between Pd and the added Au.

It should be noted that a weak shoulder peak (indicated by the arrows in Fig. 6) occurred in PdAu_{0.1}/MSN, decreased in PdAu_{0.2}/MSN, and finally disappeared for PdAu_{0.4}/MSN. We suggest that this peak may be related to the reduction of Pd ions existing as oxides, a suggestion supported by the XPS results showing that the fraction of PdO decreased with the variation in Au/Pd ratio.

It is acknowledged that the dissociative hydrogen adsorption capacity of the metal catalyst is related to the electronic structure of the metal. Combining this with the results of H₂ TPR, we suggest that the addition of Au may modify the electronic properties of Pd.

3.2. Selective hydrogenation of cinnamaldehyde

As indicated in Fig. 7, PdAu/MSN showed quite high activity toward the selective hydrogenation of CALD.

Only trace conversion was obtained for mono-Au/MSN under the given reaction conditions (0.5 MPa, 50 °C), implying low activity of Au in the hydrogenation process. For the Pd/C and Pd/MSN catalysts, the conversion of the latter (25%) was almost twice that of the former (12%), verifying the enhancement arising from the mesoporous large surface-area support. All three PdAu/MSN catalysts showed greatly enhanced activity compared with the Pd/MSN

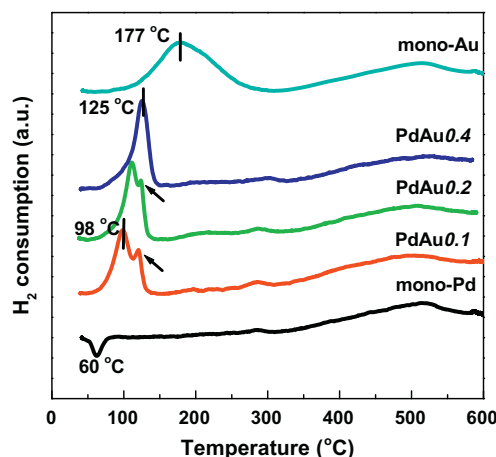


Fig. 6. H₂ TPR curves of catalysts with different metal compositions.

catalyst: the optimal PdAu_{0.2}/MSN catalyst achieved activity four and eight times higher than that of Pd/MSN and Pd/C, respectively. It is very interesting that the activities of all five catalysts were consistent with the particle sizes, hydrogen adsorption capacities, and XPS results.

As shown in Fig. 7, the selectivity of the alloy catalysts for the HALD can be improved slightly by the addition of gold. Actually, we found that the monometallic Au catalyst could reach an excellent selectivity of close to 100% at a reaction temperature of 50 °C, agreeing well with the results reported by Xu and coworkers [48,49]; however, monometallic Au catalyst showed only negligible activity toward the selective hydrogenation of cinnamaldehyde at this temperature.

Fig. 8 presents the results for the optimal PdAu_{0.2}/MSN catalyst for the selective hydrogenation of CALD at various hydrogen pressures and temperatures. The hydrogen pressure can influence activity to some extent, but has little effect on product selectivity. Clearly, the conversion increased as the hydrogen pressure increased from 0.2 to 1.0 MPa (Fig. 8a); this was because high pressure can enhance hydrogen solubility, making more hydrogen molecules accessible in the reaction medium. With further increases in the pressure, no obvious conversion increase was observed, implying the absence of a hydrogen transport limitation at higher pressures.

The hydrogenation activity was enhanced significantly with temperature increase, as shown in Fig. 8b. The conversion of CALD increased sharply from 13% to 100% when the temperature rose from 25 to 100 °C. The mass activity of Pd and Au is up to 166.6 mol h⁻¹ g_{PdAu}⁻¹ at 100 °C, thereby demonstrating the temperature-dependent behavior of the hydrogenation reaction and the high performance and thermal stability of PdAu_{0.2}/MSN.

Fig. 9 shows the Arrhenius plots of hydrogenation of CALD catalyzed by PdAu_{0.2}/MSN and Pd/MSN catalysts; two high relative lines has been obtained. The activation energies calculated from Arrhenius plots are 57 and 62 kJ mol⁻¹, respectively, further confirming the promotion of gold clearly.

The temperature also influenced the selectivity; the best selectivity (92%) of HALD for PdAu_{0.2}/MSN was obtained at 60 °C. Lower temperatures facilitate the production of completely hydrogenated hydrocinnamyl alcohol, while higher temperatures may lead to side products such as aldol condensation products.

The recyclability test for PdAu_{0.2}/MSN was carried out at 50 °C and 1 MPa hydrogen pressure. It was found that after easy separation and pretreatment, PdAu_{0.2}/MSN still could achieve a

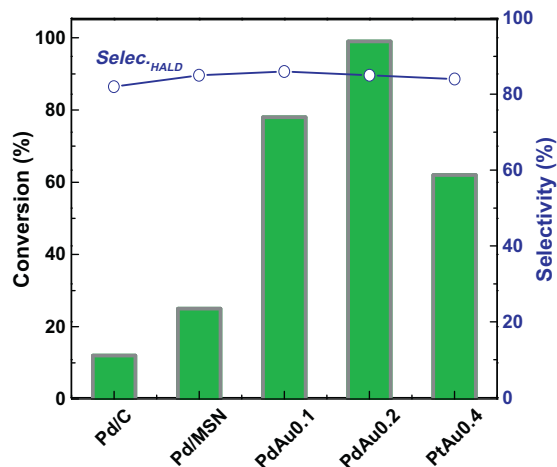


Fig. 7. Conversion and selectivity for the hydrogenation of CALD with various catalysts. Reaction conditions: 1.0 g CALD, 50 mg catalyst, 10 ml hexane as solvent, 50 °C, 0.5 MPa p_{H_2} , reaction for 1 h.

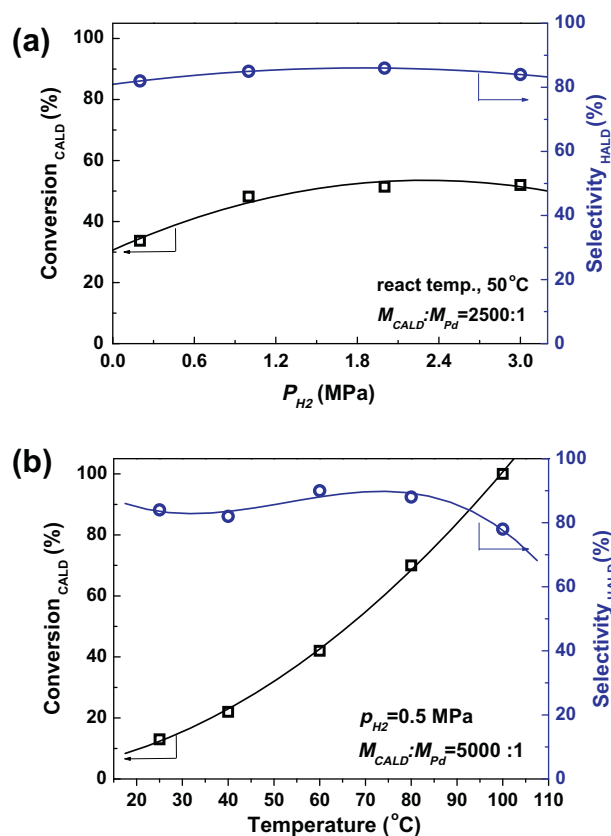


Fig. 8. Effects of hydrogen pressure (a) and temperature (b) on CALD hydrogenation performance with the PdAu_{0.2}/MSN catalyst.

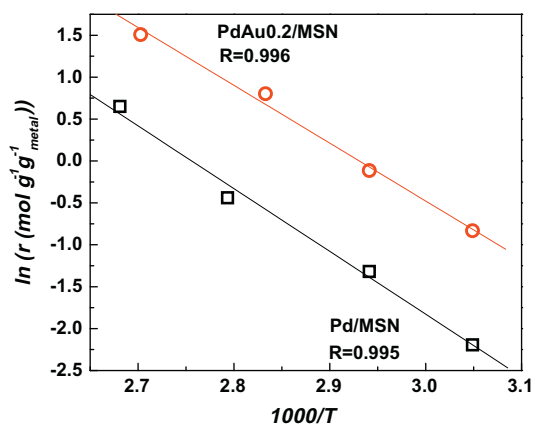


Fig. 9. Arrhenius plots for the hydrogenation of CALD over Pd/MSN and PdAu_{0.2}/MSN.

conversion of 98% and a selectivity of 85% by the fifth test, demonstrating its good deactivation resistance and recyclability. In fact, trace metal leaching (0.12 wt.%) and minimal particle sintering after the fifth test reaction contributed to its recyclability. Its excellent catalytic performance and good recyclability will make this catalyst attractive for both fundamental research and practical applications.

4. Conclusions

A high-performance PdAu bimetallic catalyst was prepared by impregnation and hydrogen reduction. It was found that the

promotion effect induced by the PdAu alloy synergistic interaction can strongly influence both the structure and the catalytic behavior of PdAu/MSN catalysts. The effect of metal composition was investigated systematically using XRD, H₂ chemisorption, XPS, and H₂ TPR. The results reveal that alloy formation plays the key role in the structure of PdAu/MSN: on the one hand, alloy formation can hinder the growth of metal particles; on the other hand, the electronic properties and compositions of active species can be tuned. The significantly improved activity can be ascribed to Pd's high dispersion and modified electronic properties. However, the intrinsic mechanism underlying these electronic properties still requires further study.

Acknowledgments

We thank the National Natural Science Foundation of China (Project s20673040, 20876062, 21076089), the Ministry of Science and Technology of China (Project 2009AA05Z119), and the Department of Science and Technology of Guangdong Province (Project 2004A11004003) for their financial support of this work.

References

- [1] M. Poliakoff, J.M. Fitzpatrick, T.R. Farren, P.T. Anastas, *Science* 297 (2002) 807–810.
- [2] P.T. Anastas, M.M. Kirchhoff, *Acc. Chem. Res.* 35 (2002) 686–694.
- [3] H. Wu, Q. Zhang, Y. Wang, *Adv. Synth. Catal.* 347 (2005) 1356–1360.
- [4] M. Lamblin, L. Nassar-Hardy, J.C. Hierso, E. Fouquet, F.X. Felpin, *Adv. Synth. Catal.* 352 (2010) 33–79.
- [5] A. Gniewek, J.J. Ziolkowski, A.M. Trzeciak, M. Zawadzki, H. Grabowska, J. Wrzyszc, *J. Catal.* 254 (2008) 121–130.
- [6] K. Mori, T. Hara, T. Mizugaki, K. Ebitani, K. Kaneda, *J. Am. Chem. Soc.* 126 (2004) 10657–10666.
- [7] C. Della Pina, E. Falletta, M. Rossi, *J. Catal.* 260 (2008) 384–386.
- [8] A. Venezia, L. Liotta, G. Pantaleo, V. La Parola, G. Deganello, A. Beck, Z. Koppány, K. Frey, D. Horváth, L. Gucci, *Appl. Catal. A* 251 (2003) 359–368.
- [9] D. Wang, A. Villa, F. Porta, L. Prati, D. Su, *J. Phys. Chem. C* 112 (2008) 8617–8622.
- [10] R. Liu, Y. Yu, K. Yoshida, G. Li, H. Jiang, M. Zhang, F. Zhao, S. Fujita, M. Arai, *J. Catal.* 269 (2010) 191–200.
- [11] M. Chen, D. Kumar, C.W. Yi, D.W. Goodman, *Science* 310 (2005) 291–293.
- [12] D.I. Enache, J.K. Edwards, P. Landon, B. Solsona-Espriu, A.F. Carley, A.A. Herzing, M. Watanabe, C.J. Kiely, D.W. Knight, G.J. Hutchings, *Science* 311 (2006) 362–365.
- [13] G.J. Hutchings, *Catal. Today* 138 (2008) 9–14.
- [14] J.K. Edwards, E. Ntainjua N, A.F. Carley, A.A. Herzing, C.J. Kiely, G.J. Hutchings, *Angew. Chem. Int. Ed.* 48 (2009) 8512–8515.
- [15] J.K. Edwards, B. Solsona, A.F. Carley, A.A. Herzing, C.J. Kiely, G.J. Hutchings, *Science* 323 (2009) 1037–1041.
- [16] L. Kesavan, R. Tiruvalam, M.H.A. Rahim, M.I. bin Saiman, D.I. Enache, R.L. Jenkins, N. Dimitratos, J.A. Lopez-Sanchez, S.H. Taylor, D.W. Knight, *Science* 331 (2011) 195–199.
- [17] B. Pawelec, A. Venezia, V. La Parola, E. Cano-Serrano, J. Campos-Martin, J. Fierro, *Appl. Surf. Sci.* 242 (2005) 380–391.
- [18] A. Venezia, R. Murania, G. Pantaleo, G. Deganello, *J. Catal.* 251 (2007) 94–102.
- [19] A. Venezia, V.L. Parola, B. Pawelec, J. Fierro, *Appl. Catal. A* 264 (2004) 43–51.
- [20] T. Wei, J. Wang, D.W. Goodman, *J. Phys. Chem. C* 111 (2007) 8781–8788.
- [21] W. Huang, J.N. Kuhn, C.K. Tsung, Y. Zhang, S.E. Habas, P. Yang, G.A. Somorjai, *Nano Lett.* 8 (2008) 2027–2034.
- [22] D. Zhao, J. Sun, Q. Li, G.D. Stucky, *Chem. Mater.* 12 (2000) 275–279.
- [23] X. Chen, S. Wang, J. Zhuang, M. Qiao, K. Fan, H. He, *J. Catal.* 227 (2004) 419–427.
- [24] G. Liu, M. Hou, T. Wu, T. Jiang, H. Fan, G. Yang, B. Han, *Phys. Chem. Chem. Phys.* 13 (2011) 2062–2068.
- [25] J.R.A. Sietsma, J.D. Meeldijk, M. Versluijs-Helder, A. Broersma, A.J. Dillen, P.E. de Jongh, K.P. de Jong, *Chem. Mater.* 20 (2008) 2921–2931.
- [26] S.H. Joo, J.Y. Park, C.K. Tsung, Y. Yamada, P. Yang, G.A. Somorjai, *Nature Mater.* 8 (2008) 126–131.
- [27] E. Ghedini, F. Menegazzo, M. Signoretto, M. Manzoli, F. Pinna, G. Strukul, *J. Catal.* 273 (2010) 266–273.
- [28] Z. Ma, S. Dai, *Nano Res.* 4 (2011) 3–32.
- [29] A.J. Plomp, H. Vuori, A.O.I. Krause, K.P. de Jong, J.H. Bitter, *Appl. Catal. A* 351 (2008) 9–15.
- [30] H. Ma, L. Wang, L. Chen, C. Dong, W. Yu, T. Huang, Y. Qian, *Catal. Commun.* 8 (2007) 452–456.
- [31] J.P. Tessonnier, L. Pesant, G. Ehret, M.J. Ledoux, C. Pham-Huu, *Appl. Catal. A* 288 (2005) 203–210.
- [32] C. Pham-Huu, N. Keller, G. Ehret, L.C.J. Charbonniere, R. Ziessel, M.J. Ledoux, *J. Mol. Catal. A Chem* 170 (2001) 155–163.
- [33] P. Gallezot, D. Richard, *Catal. Rev.* 40 (1998) 81–126.
- [34] Q. Fan, Y. Liu, Y. Zheng, W. Yan, *Front. Chem. Eng. China* 2 (2008) 63–68.
- [35] X. Yang, L. Du, S. Liao, Y. Li, H. Song, *Catal. Commun.* (2011) 29–33.
- [36] Y. Han, L. Zhao, J.Y. Ying, *Adv. Mater.* 19 (2007) 2454–2459.
- [37] G. Alvez-Manoli, T.J. Pinnavaia, Z. Zhang, D.K. Lee, K. Marín-Astorga, P. Rodriguez, F. Imbert, P. Reyes, N. Marín-Astorga, *Appl. Catal. A* 387 (2010) 26–34.
- [38] A. Sarkany, O. Geszti, G. Safran, *Appl. Catal. A* 350 (2008) 157–163.
- [39] G. Zhang, Y. Wang, X. Wang, Y. Chen, Y. Zhou, Y. Tang, L. Lu, J. Bao, T. Lu, *Appl. Catal. B* 102 (2011) 614–619.
- [40] A. Lee, C. Ellis, K. Wilson, N. Hondow, *Catal. Today* (2010) 243–249.
- [41] H. Borchert, E.V. Shevchenko, A. Robert, I. Mekis, A. Kornowski, G. Grübel, H. Weller, *Langmuir* 21 (2005) 1931–1936.
- [42] H. Natter, M. Schmelzer, M.S. Löffler, C. Krill, A. Fitch, R. Hempelmann, *J. Phys. Chem. B* 104 (2000) 2467–2476.
- [43] B. Lee, Z. Ma, Z. Zhang, C. Park, S. Dai, *Micropor. Mesopor. Mater.* 122 (2009) 160–167.
- [44] J. Pritchard, L. Kesavan, M. Piccinini, Q. He, R. Tiruvalam, N. Dimitratos, J.A. Lopez-Sanchez, A.F. Carley, J.K. Edwards, C.J. Kiely, G.J. Hutchings, *Langmuir* 26 (2010) 16568–16569.
- [45] A.A. Herzing, M. Watanabe, C.J. Kiely, J. Edwards, M. Conte, Z.R. Tang, G.J. Hutchings, *Faraday Discuss.* 138 (2008) 337–351.
- [46] K. Qian, W. Huang, *Catal. Today* 164 (2011) 320–324.
- [47] C.W. Chou, S.J. Chu, H.J. Chiang, C.Y. Huang, C. Lee, S.R. Sheen, T.P. Perng, C. Yeh, *J. Phys. Chem. B* 105 (2001) 9113–9117.
- [48] H. Shi, N. Xu, D. Zhao, B.Q. Xu, *Catal. Commun.* 9 (2008) 1949–1954.
- [49] K. Sun, Y. Hong, G. Zhang, B.Q. Xu, *ACS Catal.* 1 (2011) 1336–1346.